New Journal of Physics
The open–access journal for physics

Electrical and optical characterization of the plasma needle

I E Kieft, E P v d Laan and E Stoffels

Department of Biomedical Engineering, Eindhoven University of Technology, PO Box 513, 5600 MB Eindhoven, The Netherlands
E-mail: E.Stoffels.Adamowicz@tue.nl and i.e.kieft@tue.nl

New Journal of Physics **6** (2004) 149
Received 22 July 2004
Published 28 October 2004
Online at http://www.njp.org/
doi:10.1088/1367-2630/6/1/149

Abstract. The plasma needle is a source to create a non-thermal radiofrequency plasma at atmospheric pressure. To improve the ease of working on biological samples, a flexible plasma probe was designed. In the new configuration, the needle was confined in a plastic tube through which helium flow was supplied. The new set-up was characterized by impedance measurements and emission spectroscopy. Impedance measurements were performed by means of an adjustable matching network; the results were modelled. The discharge was found to be entirely resistive; the measured voltage was in the range 140–270 V_{rms} and it was in excellent agreement with model results. From the resistance, the electron density was estimated to be $10^{17}\,m^{-3}$.

Optical measurements showed substantial UV emission in the range 300–400 nm. Active oxygen radicals ($O^{\bullet}$ and $OH^{\bullet}$) were detected. Furthermore, the influence of helium flow speed was investigated. At low flow speeds, the density of molecular species in the plasma increased.

UV emission and density of active species are important factors that determine the performance of plasma in the treatment of biological materials. Therefore, the new characterization will help us to understand and optimize the interactions of atmospheric plasma with cells and tissues.

PII: S1367-2630(04)83748-0
© IOP Publishing Ltd and Deutsche Physikalische Gesellschaft

Contents

1. Introduction

The plasma needle is a type of non-thermal atmospheric glow discharge; it has a single-electrode configuration and is operated in helium [1]. Important properties of this type of plasma are that it operates near room temperature, allows treatment of irregular surfaces and has a small penetration depth. These characteristics give the needle great potential for use in the biomedical field. This work is aimed at studying cells and bacteria that are treated with the plasma. Experiments have already shown that the plasma needle is capable of bacterial decontamination [2] and of localized cell removal without causing necrosis to the treated or neighbouring cells [3]. Areas of detached cells were made with a diameter of 0.1 mm, which indicates that the precision of the treatment can be very high. It is believed that plasma particles, such as radicals and ions, and also emitted UV light, interact with the cell membranes and cell adhesion molecules and therefore cause detachment of the cells [3]. The penetration of the plasma radicals in liquid was tested [4], and densities in the μM range were observed.

In this paper, we characterize a new configuration of the plasma needle, by describing its electrical set-up and by studying light emission. The design of the needle was changed to improve the ease of working and to allow treatment of large-sized objects. This was not possible in the former configuration because the needle was enclosed in a box [1], which meant that specimens had to be placed inside. The box had dimensions of $10 \times 10 \times 10$ cm and it was filled with helium after the specimens had been put in, which took 30 s to 1 min. In the new design, this box is replaced by a tube, through which helium flow is directed coaxially with the needle. Near the needle tip, helium mixes with air. The percentage of air at this point has been determined by Raman scattering to be in the range 0.1–1% [4]. This way, a plasma is created that is at first sight comparable with the high-frequency plasma pencil [5] and the plasma-energized jet [6]. However, the micro-plasma generated by the plasma needle has a gas temperature much closer to room temperature than in other designs and is thus more suitable for the intended tissue treatment.

To electrically characterize the plasma, the voltage at the needle as well as the power dissipated by the plasma were determined. Furthermore, we measured the impedance of both the plasma and the matching network.

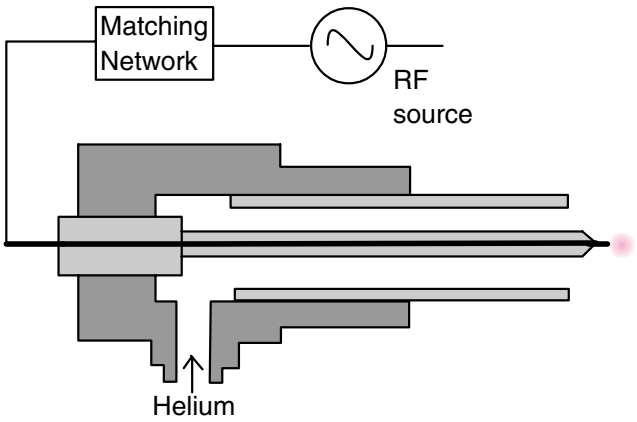

Figure 1. Schematic drawing of the experimental set-up. The electrode wire is fixed in a stainless steel holder and insulated by a glass tube, leaving only the tip exposed. The outer Perspex tube surrounding the wire can be moved horizontally.

The method used to obtain the impedance of the RF discharge that was applied here was based on transmission line theory: a variable matching network was inserted to match the impedance of the plasma set-up with the internal impedance of the power supply [7, 8]. Firstly, the impedance of the matching network was determined and put into a model. The model allowed calculation of the impedance of the discharge. The plasma appeared to be entirely resistive: no capacitive component was found. The power dissipated by the plasma was found to be dependent on the distance between the plasma needle and the treated surface. This property might be used as a measurement tool for automatic control of the position of the needle relative to a surface.

The light emission by the plasma was studied by optical emission spectroscopy. This method is commonly used for plasma analysis [9]–[11]. The emission spectra are used to investigate possible UV emission and the composition of the plasma. UV emission and radicals are important for the application of plasma to biological samples because both are known to be potentially damaging to cells; they can induce programmed cell death (apoptosis) [12]–[14].

Emission spectroscopy was also used to investigate the effect of a change in helium flow rate. Under all conditions, UV radiation was mainly emitted in the region between 305 and 390 nm; the species that could be detected were $OH^{\bullet}$, $O^{\bullet}$, N_2^+, N_2 and He. An abrupt increase (jump) in the intensity of the light emission was found when the applied voltage was increased while keeping the other parameters constant. This jump could indicate a transition to another plasma mode.

2. Method

2.1. Plasma needle

A schematic drawing of the plasma needle (figure 1) shows the plasma at the sharp end of a metal-alloy pin (diameter 0.3 mm). The typical size of the plasma glow was 2 mm in diameter (figure 2).

The metal pin was inserted coaxially in a Perspex tube; it protruded from the stainless steel holder by 1.5 cm. The total length of the needle was about 8 cm. To prevent a discharge along the entire pin, it was insulated by glass. Helium flowed through the plastic tube at the rate of

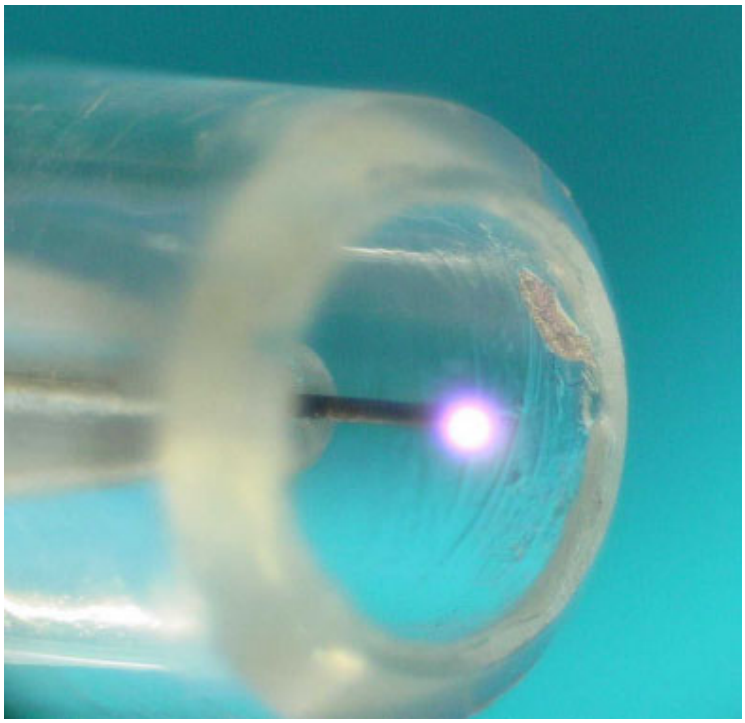

Figure 2. Plasma generated by the plasma needle. The plasma appeared as a pink glow with a diameter of approximately 1 mm at the tip of the needle.

2 litres min^{-1} unless stated otherwise. The flow rate was regulated with a mass flow controller from Brooks series 5850E. Because the inner diameter of the Perspex tube was 5.5 mm, this flow rate resulted in a velocity of 1.4 m s^{-1}. The helium flow was mixed with a small amount of air near the tip. Moving the Perspex tube relative to the fixed needle regulated the percentage of air. In the study described here, the end of the tube reached as far as the needle tip.

The RF signal was generated by a waveform generator Hewlett Packard 33120A and amplified by an RF amplifier model 75AP250 by Amplifier Research. From the amplifier, the signal was directed to a home-built matching network, which is described in a later section.

A bidirectional power meter was placed in-between the amplifier and the matching network to measure the forward and reflected power. The meter was the PM 2002 obtained from Amplifier Research with directional couplers also from Amplifier Research. A voltage probe P6150A by Tektronix was attached to the feed-through of the needle when voltage measurements were carried out. The probe was a 1000 × attenuator with 100 MΩ resistance and 3 pF capacitance.

2.2. Impedance measurements

In order to measure the impedance of both the metal pin and the discharge, first the impedance of the matching network (figure 3) had to be determined. The matching network had to be characterized carefully, and thus it was necessary to know the components of the network as well as its stray impedances. To determine these stray impedances, the method described by Bakker *et al* [8] was used, which is based on the reflection of power by the matching network. To use this method for our set-up, it was necessary to first adapt the matching network: it was made adjustable and more stable.

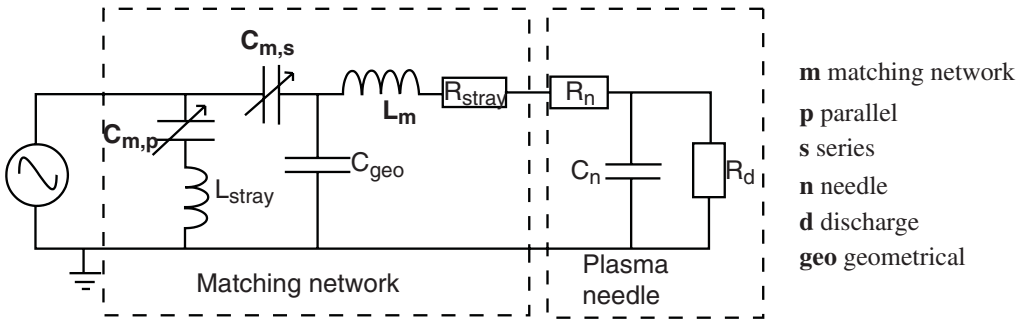

Figure 3. Components of the matching network and of the plasma needle.

Then a stepwise approach was followed to determine the discharge impedance: (1) the matching network was short-circuited and stray impedances were calculated; (2) the load impedance (the plasma needle) was connected and the network was matched; (3) from the settings, the plasma impedance was calculated. A short-circuit (used in step 1) is a fixed load with zero real and imaginary values and it is independent of voltage and frequency.

For step 1, the components of the matching network were identified with the assumed stray impedances (figure 3). The basic components that were physically put into the network were the coil L_m and the capacitances $C_{m,s}$ and $C_{m,p}$. These capacitances were Jennings tuning vacuum capacitors with very high quality factors (Q). Therefore, they were assumed not to have any intrinsic stray impedance. The capacitors' impedances were measured when they were fully disconnected; the measured values were then put into the model. Because of the high Q values, the capacitances could be measured at 1 kHz and the obtained values were still reliable for use at 13.56 MHz. The impedances of these capacitances were measured with an automatic RCL meter by Fluke (model 6303A) at 1 kHz. Depending on the plasma load, $C_{m,s}$ and $C_{m,p}$ varied between 500 and 520 pF and 290 and 310 pF respectively. The inductance of the coil was determined to be 3.4 μH at 3.2 MHz. However, because the coil did not have a high Q factor, at higher frequencies the inductance deviated from the value measured at 3.2 MHz and thus the latter could only be used as an indication for the model.

Besides the impedances of the basic components, stray impedances were taken into account. These were called L_{stray} and R_{stray}. The impedance L_{stray} originated from the wires that were connected to the capacitor $C_{m,p}$, because these wires had a small inductance. Since the wires were very flat, the resistive skin effect was neglected. The stray inductance from the wires that connected $C_{m,s}$ and L_m was included in L_m in the model. In the model of the matching network, a capacitance C_{geo} had to be added because $C_{m,s}$ was located very close to the grounded case and this gave an extra capacitive impedance.

To determine the stray impedance values, we used equation (1), which stated that the reflection of power is a function of the impedance.

$$\frac{P_{ref}}{P_{forw}} = \left| \frac{Z - 50\,\Omega}{Z + 50\,\Omega} \right|^2 . \tag{1}$$

The forward and reflected power were measured with the bidirectional power meter as a function of $C_{m,p}$. For these measurements, the network was matched at 13.56 MHz and $C_{m,p}$ was varied,

whereas $C_{m,s}$ was kept constant. The values of the stray impedances were determined by fitting the function to the measured values.

This was followed by step 2: Connecting the load impedance. The settings of $C_{m,s}$ and $C_{m,p}$ in the matched situation with load were recorded, and from this the load impedance was determined. The load impedance was divided into two components: the needle itself and the discharge. The impedance of the needle was found when the plasma was turned off. It had a capacitive and a resistive component. The impedance of the discharge had only a resistive part. The transmission line that connected the matching network to the needle transformed the load impedance. This transformation [15] is given by

$$Z_{load} = Z_0 \frac{Z_{needle+discharge} + Z_0 j \tan(\beta l)}{Z_0 + Z_{needle+discharge} j \tan(\beta l)}, \tag{2}$$

where Z_0, is the impedance of the transmission lines. Both Z and the internal impedance of the RF source, are non-imaginary and fixed at 50 Ω, β is the phase constant: it is the imaginary part of the propagation constant and l is the length of the coaxial cable from the matching box to the needle system, which was, in our set-up, 0.25 m with $\beta = 0.43\,\mathrm{rad\,m^{-1}}$.

2.3. Light emission

To analyse light emission, we performed spectroscopy measurements; the data obtained were used to determine the plasma composition. The helium flow rate was varied to investigate the influence of flow velocity on the emission and thus on the composition of the plasma.

For the spectroscopy, two types of spectrometers were used. The first was the JobinYvon H25, which had a good resolution (peaks 1 nm apart could be distinguished). For focusing, a quartz lens was used with a focal length of 0.25 m. The grating of the spectrometer had 1500 lines per mm. The image produced by the spectrometer was taken with an intensified charge-coupled device (iCCD) camera (Andor DH534) at a cooling temperature of −35 °C. The exposure time was set at 0.7 s and the gate width at 2000 ns. The accumulation number we used was 100. The quantum efficiency of the CCD camera was greatly reduced for wavelengths above 800 nm, where the efficiency was at least a factor 10 lower than that in the range 300–500 nm.

For quicker but lower-resolution (peaks 5 nm apart could be distinguished) measurements, an Ocean Optics HR2000 was used. The fibre was 2 m long. Through the fibre the signal was greatly attenuated (>20%) for wavelengths below 300 nm and from 900 to 1000 nm. The numerical aperture of the fibre was 0.22, which equalled a whole acceptance angle of 24.8°. A collimating quartz lens was placed in front of the fibre to couple parallel beams into the fibre. The diameter of this lens was 5 mm, which enables us to view the entire plasma at once.

Light intensity measurements were performed with a photodiode UV50 of UDT Sensors. The sensor had a sensitivity range of 200–1100 nm with a peak at 800 nm.

3. Results and discussion

3.1. Impedance measurements

In the previous section, we explained that, before impedance measurements could be done on the discharge, first the matching network needs to be known. To map the network, a short-circuit

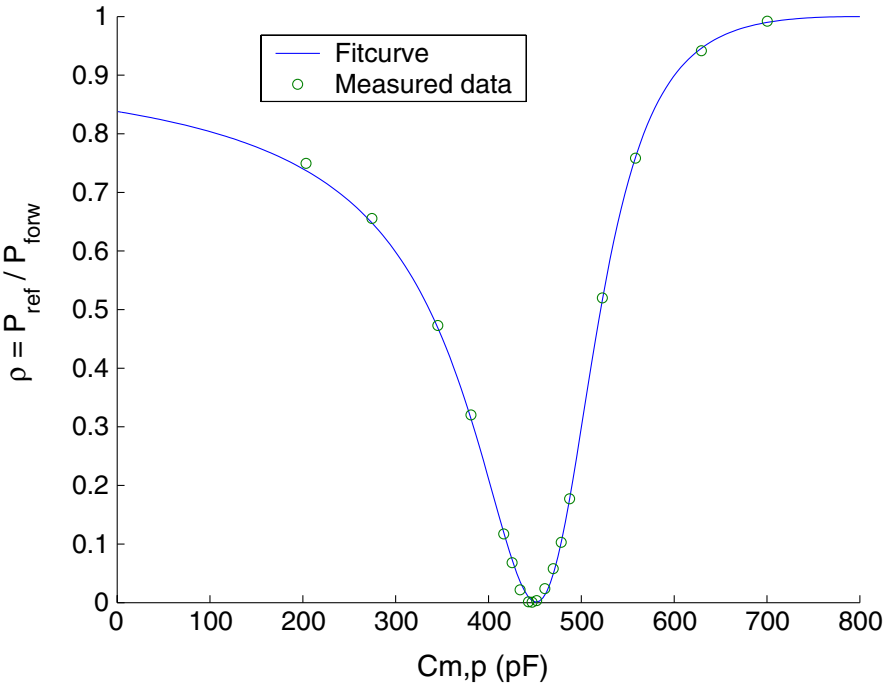

Figure 4. The reflection coefficient in relation to $C_{m,p}$ and the curve fit made to determine stray impedances.

Table 1. Capacitance settings for the matching network mapping and the determined stray impedance values.

Component	Value
$C_{m,p}$	446.9 pF
$C_{m,s}$	22.30 pF
C_{geo}	21.02 pF
R_{stray}	0.6728 Ω
L_m	3.018 μH
L_{stray}	14.65 nH

was used to close it. Then the reflection coefficient, which is the reflected power divided by the forward, was measured as a function of $C_{m,p}$ (figure 4). $C_{m,s}$ was kept at a constant value (22.30 pF) during these measurements.

In the matched situation, the reflected power was about 50 μW, which was very small compared with the forward power of 1 W. The obtained data were used to make a model of the matching network and thus determine the stray impedance values (table 1). This reflection coefficient calculated with the model fitted the measured coefficient well, with a dataset correlation of 0.9998.

Because the components of the matching network were now known, we could determine the plasma needle characteristics with a high precision. As was explained in the section 2, the impedance of the plasma needle was divided into a resistive and a capacitive component of the needle itself and a resistive component of the discharge. The resistance of the needle without

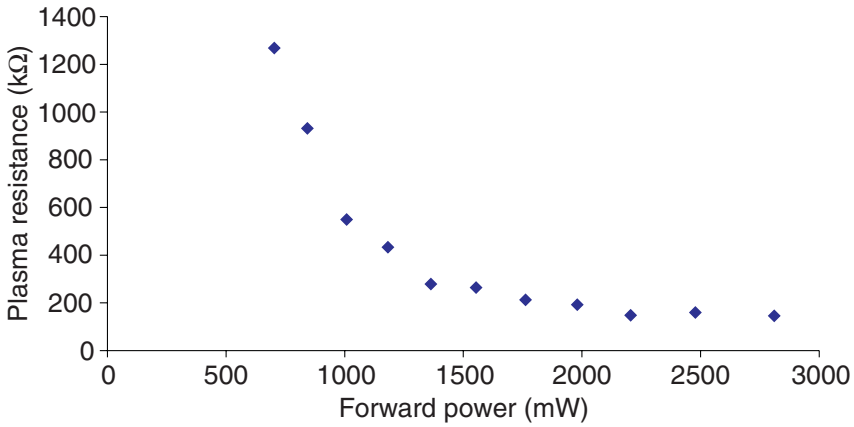

Figure 5. Discharge impedance as a function of forward power. The impedance ranged from 100 to 1200 kΩ.

discharge was 1.1 Ω, and its capacitance was 28.8 pF. The impedance of the discharge depends on external parameters like the forward power (figure 5), and on the distance between the needle and the treated surface. Without a nearby surface, the plasma impedance was calculated to be in the range 100–1200 kΩ. The resistance of the plasma decreased with increase in forward power. The power dissipated in the discharge ranged from tens of mW to a few hundred mW. The power efficiency increased from a few per cent to 20% when the forward power was increased from 700 mW to 3 W. We also observed that the size of plasma increased with increasing power (roughly from 1 to 4 mm in diameter).

Knowing the resistance of the discharge and the size of the glow, we can estimate the electron density, since the resistance of the plasma is mainly determined by collisions of electrons with neutrals. For a weakly ionized plasma, the conductivity σ (in $\Omega^{-1}\,\mathrm{m}^{-1}$) depends mostly on the degree of ionization n_e/n_a, with n_e being the electron density and n_a the neutral density. Equations (3) and (4) [16] can be used to estimate n_e.

$$\sigma = \frac{n_e e^2}{m_e \nu_{ea}}, \tag{3}$$

$$\nu_{ea} = n_a \sigma_{ea} \upsilon_e. \tag{4}$$

Firstly, we use equation (4) to calculate the collision frequency ν_{ea}. The average speed of the electrons, υ_e is taken to be $0.84 \times 10^6\,\mathrm{m\,s}^{-1}$, because we can assume the average electron temperature to be 2 eV for an atmospheric helium plasma [17, 18]. At this speed, the cross-section σ_{ea} is $5 \times 10^{-20}\,\mathrm{m}^2$ for collisions between electrons and neutrals [16]. With the density of the gas at atmospheric pressure $n_a = 2.5 \times 10^{25}\,\mathrm{m}^{-3}$, the ν_{ea} was calculated to be about $1.6 \times 10^{12}\,\mathrm{s}^{-1}$.

The conductivity in equation (3) was calculated from the size of the plasma and the corresponding resistance. The size of the plasma was determined from the size of the glow, which was assumed to be spherical. The resulting electron density was found to be $10^{17}\,\mathrm{m}^{-3}$. The conductivity and thus the electron density varied as a function of the forward power, as shown in figure 6. This figure indicated that, when the forward power exceeded 2000 mW, the

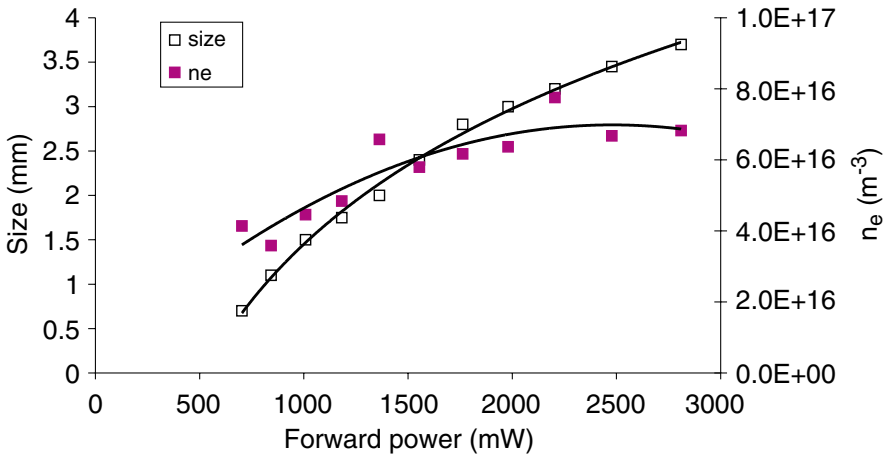

Figure 6. Diameter of the plasma and the estimated electron density.

plasma expanded in volume, but the electron density remained almost constant. So it seems that the chemical activity of the discharge remained the same while the glow increased in size.

The electron density of $10^{17}\,\mathrm{m}^{-3}$ seems reasonable if we compare it with the electron density of another non-thermal RF plasma at atmospheric pressure with helium as feed gas: the atmospheric-pressure plasma jet (APPJ). The density of the α-mode discharge of the APPJ was $3 \times 10^{17}\,\mathrm{m}^{-3}$ [19], which is equivalent to the density we found for the plasma needle.

Using the model that was developed for the impedance calculations, we calculated the voltage at the connector of the transmission line to the plasma needle. Thus, the fall in voltage was calculated over both the resistance of the needle and the resistance of the discharge. For this calculation, we used the forward power at the power meter to determine the start values V_0 and I_0. In a matched situation, the impedance of the system was non-imaginary and 50 Ω at the input of the matching network. The voltage at the load could then be determined from these start values, because all impedance components were known, including the transmission line from the matching network to the load (see equation (2)). It was not necessary to take into account the transmission line from the power meter to the matching network, because this line was terminated by 50 Ω in the matched situation and therefore it did not influence the amplitude of voltage. The calculated voltage appeared to agree with the measured voltage (figure 7). The minimum voltage needed to sustain the plasma was just below 140 V. This is higher than that in the old configuration, where it was as low as 90 V [3].

To ensure good reproducibility and high precision, it is important to learn how the plasma characteristics change during surface treatments. To this end, the needle voltage was measured when its tip was approaching a surface. The surfaces that were used during voltage measurements were: plastic (non-conducting), demineralized water (conductivity, $2\,\mu\mathrm{S\,cm}^{-1}$) and aluminium (conductivity, $0.4\,\mathrm{MS\,cm}^{-1}$) [20]. The conductivity of water was closest to that of the biological material (for most tissues, in the range of $\mathrm{mS\,cm}^{-1}$) [21]. Only when the surface was (partly) conducting, the voltage decreased during the approach. The first influence on the discharge could be noticed at a distance of 5 mm; from that point, the effect continuously increased. The size of the plasma was about 2 mm in diameter, which means that the charged particles from the active plasma zone had to pass about 3 mm to reach the grounded surface. The voltage decrease was quite strong: a decline from 190 to 150 V for the liquid and aluminium surfaces. When

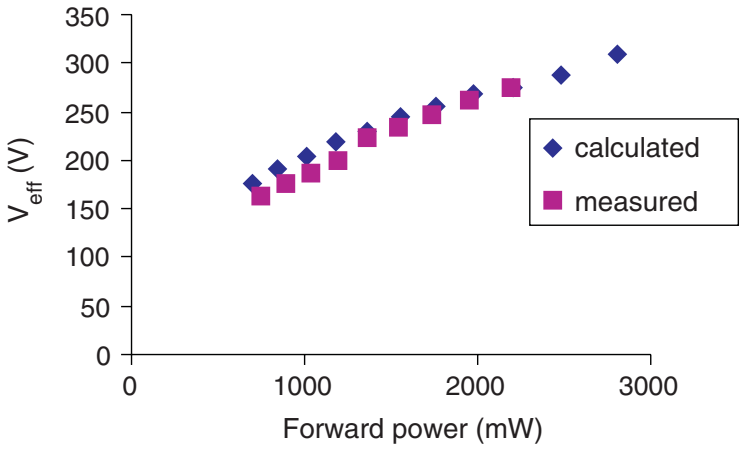

Figure 7. Measured and calculated voltage at the connector of the plasma needle.

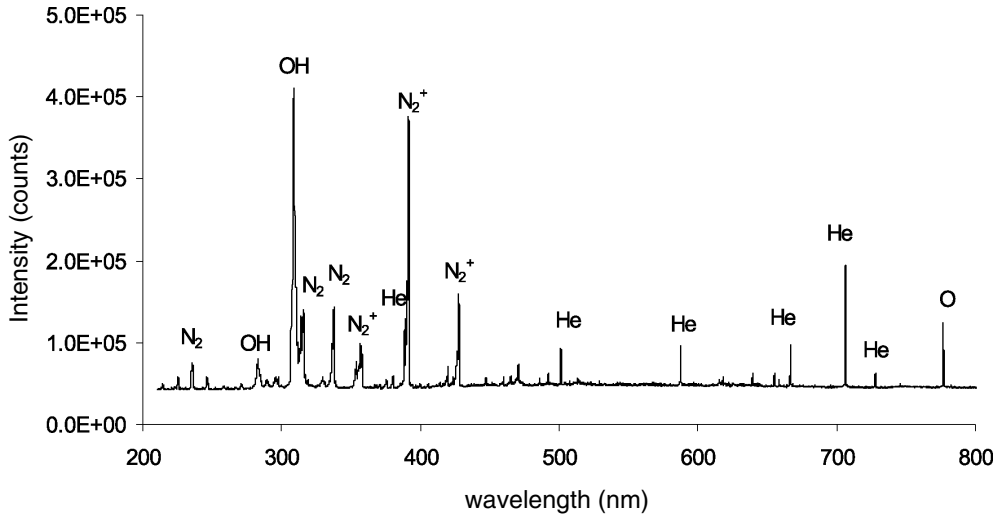

Figure 8. Emission spectrum for the plasma needle. Emission lines were ascribed to He, N_2, N_2^+, $OH^\bullet$ and $O^\bullet$. Note that sensitivity drops notably for wavelengths greater than 750 nm.

the aluminium surface was approached to about 1 mm, the voltage dropped to 125 V, and the plasma became arc-like in appearance. Upon approaching the surfaces, the net power dissipated in the matching network and the plasma needle slightly increased. This relation can be used as an indicator of the distance from treated surface. This is of importance in the treatment of biological tissues, where doses of plasma irradiation must be carefully controlled. For precise and well-reproducible treatment, the needle-to-surface distance should be kept constant.

3.2. Light emission

Light emission is monitored to detect possible UV emission and to determine the composition of the plasma. From the emission spectrum (figure 8), the discharge composition can be studied by ascribing the emitted lines to specific excited atoms and molecules. We must keep in mind

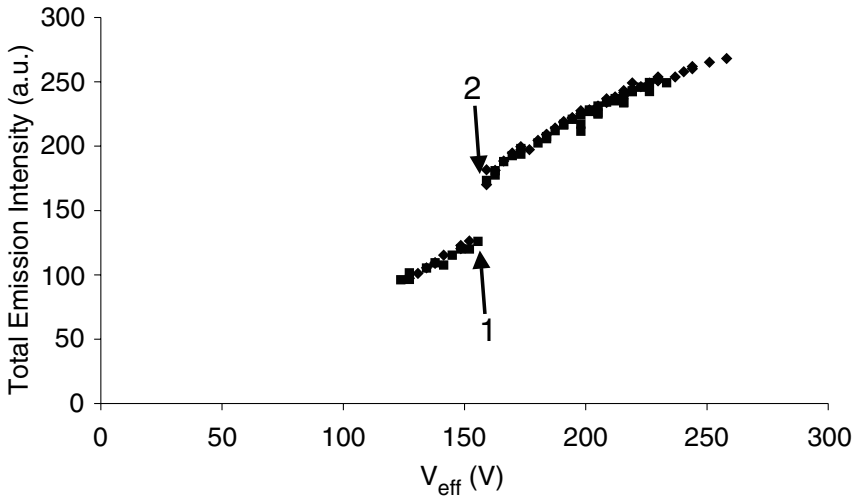

Figure 9. At a certain voltage increase supplied to the needle, a jump in light emission was observed using a photodiode. This could indicate a transition in plasma mode.

that only weak emission bands have been reported for ozone in the scientific literature [22], so ozone is not likely to be detected.

Emission lines could be ascribed to He, N_2, N_2^+, $OH^\bullet$ and $O^\bullet$. The 3064 Å ($A^2\Sigma^+ \rightarrow X^2\Pi$ transition) emission of $OH^\bullet$ is found generally when water vapour is present, as is the case in our open-air system. The first negative system of N_2^+ ($B^2\Sigma_u^+ \rightarrow X^2\Sigma_g^+$) can be observed, as was expected in the presence of excess helium [22]. For N_2 we see the second ($C^3\Pi \rightarrow B^3\Pi$) and fourth ($D^3\Sigma^+ \rightarrow B^3\Pi$) positive systems. The second positive system appears readily in discharges containing nitrogen [22]. Interestingly, the intensity of the nitrogen lines was not dominant over the helium lines. This indicated that the discharge was mainly based on helium, and the blending of nitrogen was low.

For an atmospheric helium plasma, it is not possible to determine the electron temperature from the emission spectrum [17]. The relative densities of excited states, obtained from the spectra, can be used to make Saha plots [18], but these plots yield only the excitation temperature, which is not directly dependent on the electron temperature. This is because, in a non-equilibrium system, there is a drain of charged particles that leads to an overpopulation of the lower atomic states with respect to the Saha balance [18]. Electron temperature in such systems must be determined in another way, e.g. by means of Thomson scattering. The fact that helium is the lightest noble gas having high ionization potential results in high T_e and low n_e. As mentioned before, the typical electron temperature in atmospheric helium plasma is around 2 eV [17, 18].

Subsequently, we studied the relation between the applied voltage and the total (wavelength integrated) light emission, recorded by a photodiode. The total light emission was assumed to be an indicator of the size of the plasma. A sudden increase (jump) in light emission intensity was observed when the voltage and input power were raised above a certain threshold value (figure 9).

This sudden increase in emission when voltage was raised above 160 V_{rms} could indicate a change in plasma mode, which is usually followed by a change in electron temperature. To study this behaviour further, we analysed spectra taken at points 1 and 2 in figure 9 made with the Ocean Optics HR2000 (sensitivity between 200 and 600 nm). Going from points 1 to 2, the

total intensity of the spectrum increased by a factor 6, whereas the intensity of the helium line at 588 nm increased by a factor 12; the emission of the $OH^{\bullet}$ and N_2^+ lines increased approximately at the same rate as the total intensity. The intensities of the N_2 lines decreased relative to the total intensity. This indicates that, in the low-voltage mode (<160 V), the plasma is sustained mainly by ionization of the impurities. This feature of the plasma needle can be understood, because the molecular impurities are relatively easy to excite and ionize, while efficient ionization of helium requires a certain threshold voltage.

Shi *et al* [23] described several modes of RF atmospheric plasmas that were similar to the alpha mode. In addition to the generally known alpha mode, they introduced the normal glow mode and the recovery mode. These modes, similar to the alpha mode, had a diffuse and uniform appearance, and for both modes the ionized gas was close to room temperature. The two modes we observed in figure 9 were both at low temperature and were most probably of the alpha-mode type. However, because the plasma needle has a unipolar configuration, we cannot directly compare the observed modes with those of Shi *et al* [23], and more research is needed to determine the exact plasma modes of the needle.

3.3. Influence of helium flow speed

The advantage of decreasing helium flow rate is that it is cost-saving, and it would be practical for use in small openings and for vulnerable tissues. However, due to the lower flow speed, more air will diffuse into the discharge and this will change its characteristics. The ionization potential of nitrogen is 15.58 eV, whereas it is 24.59 eV for helium, and therefore nitrogen will become the predominantly ionized gas. The disadvantage of a lower flow speed is an increase in gas temperature, because the heat loss due to convection is lower. Furthermore, the heat conductivity of nitrogen is lower than that for helium (24×10^{-3} versus 144×10^{-3} W m^{-1} K^{-1}).

To investigate the effect of helium flow on the composition of the plasma, the flow was reduced from the standard 2 litres min^{-1} to 0.5 litre min^{-1} and the emission spectra were analysed. This flow reduction meant that the flow speed varied from 1.4 to 0.35 m s^{-1}. At lower flow rates, the plasma became unstable. The power needed to sustain the plasma decreased slightly from 3.8 W forward power to 3.7 W, with the reflected power decreasing from 26 to 6 mW. At first sight, this may seem illogical, because the supply of helium was lower and more impurity (molecules) was diffusing in, thereby causing a loss of electron energy due to excitation and dissociation of the molecules. However, the nitrogen molecules were easier to ionize owing to their lower ionization potential.

The spectrometer used for these measurements has a sensitivity range of 200–600 nm, which means that some helium lines and the 777 nm atomic oxygen line were not included.

When the helium flow was turned down, the total spectral intensity increased. This was mainly due to a substantial increase in N_2 emission (figure 10). Because the strongest nitrogen lines were below 400 nm, the emission of UV light increased. Unfortunately, at low flow rates, nitrogen lines significantly interfered with the $OH^{\bullet}$ lines and an increase in these lines could not be linked directly to a rise of OH radical density. Thus, we were unable to describe the behaviour of the OH radicals. Our previous study using fluorescent probes [4] indicated that the oxygen-radical density decreased when impurities such as oxygen or air were admixed with helium. However, in those measurements [4], the concentration of molecular species was in the 0.1–1% range. Such amounts of oxygen led to a drastic reduction of plasma activity (e.g. decrease of electron density), which was expressed by suppression of helium line emission. This

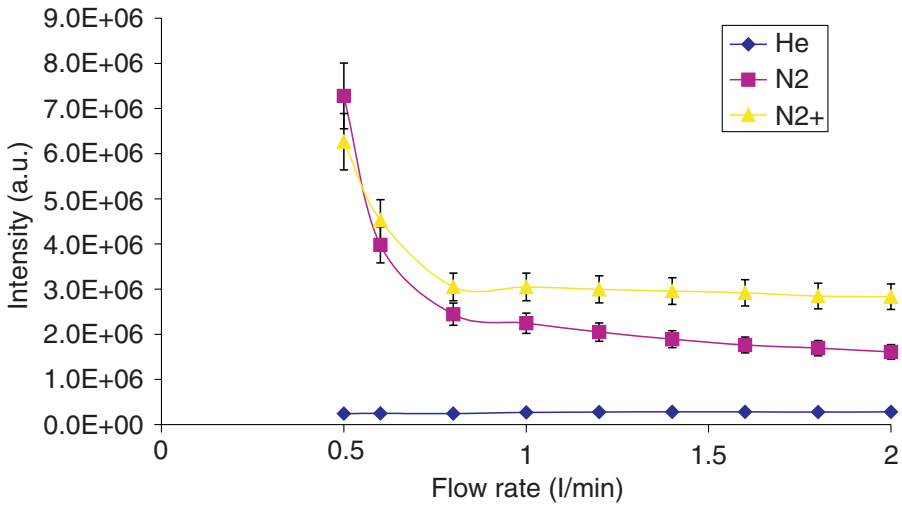

Figure 10. Intensity dependence on the helium flow rate for He, N_2 and N_2^+. There is a large increase in emission for low flow speeds, mainly for nitrogen lines.

was not the case in the present experiment, because helium line emission remained constant even at low flow rates (figure 10). Therefore we can tentatively conclude that the diffusion of air and water vapour into the plasma results in very low concentrations of nitrogen/oxygen molecules (<0.1%). At such low concentrations of air, reasonable densities of excited species can be reached, while there is no unfavourable influence on the plasma. For optimal conditions of treatment, the concentration of reactive species should be maximized. This may be achieved by careful admission of low amounts of specific gases into the helium flow (in the 0.1% range) and also by reduction of the helium flow rate, which leads to enhancement of the density of excited nitrogen species.

4. Conclusions

In this paper, we described both optically and electrically the characteristics of the plasma needle in a new design. This design had recently been adjusted so that cell treatments need not have to be performed inside a box. A model was made to characterize the plasma needle impedance. Using this model, the discharge was found to be entirely resistive, ranging from 100 to 1200 kΩ. This allowed us to make an estimation of the electron density: 10^{17} m^{-3}. The electron density increased with increase in forward power until it saturated at about 2 W. At power levels above 2 W, the electron density remained relatively constant, whereas the size of the plasma increased.

Optical characterization was performed using emission spectroscopy. We found an abrupt increase in the emission intensity when the voltage at the needle was 160 V. This could indicate a transition into another plasma operation mode. In the low-voltage mode (140–160 V), the spectrum was dominated by N_2, N_2^+, $OH^\bullet$ and $O^\bullet$, while at voltages higher than 160 V relatively more helium line emission was detected.

The presence of UV emission is an important factor in the treatment of biological materials because of possible damage to cells. In our plasma, UV emission was found in the region between 250 and 400 nm, but the highest intensities were between 305 and 390 nm. At these wavelengths, the damage to cells and tissues is limited [24].

The influence of the helium flow velocity was investigated for the purposes of cost saving and convenience of operation in small openings and on vulnerable tissues. A reduction of helium flow influenced the spectrum: nitrogen lines became much more prominent. This effect became significant when the flow was reduced to below 0.8 litre min^{-1}. A disadvantage of the nitrogen admixture may be an increase in gas temperature due to the lower heat conductivity of N_2. The characterization of the needle allows a better control of the plasma source and helps to optimize plasma conditions in the treatment of biological samples.

Acknowledgments

The authors thank Bart Broks for his useful comments. This research was supported by the Dutch Organization for Scientific Research (NWO).

References

[1] Stoffels E, Flikweert A J, Stoffels W W and Kroesen G M W 2002 *Plasma Sources Sci. Technol.* **11** 383
[2] Sladek R E J, Stoffels E, Walraven R, Tielbeek P J A and Koolhoven R A 2004 *IEEE Trans. Plasma Sci.* **32** 1540
[3] Kieft I E, Boers J L V, Caubet-Hilloutou V, Slaaf D W and Stoffels E 2004 *Bioelectromagnetics* **25** 362
[4] Kieft I E, van Berkel J J B N, Kieft E R and Stoffels E 2004 *Plasma Processes Polym.* at press
[5] Janca J, Klima M, Slavicek P and Zajickova L 1999 *Surf. Coat. Technol.* **116–119** 547
[6] Toshifuji J, Katsumata T, Takikawa H, Sakakibara T and Shimizu I 2003 *Surf. Coat. Technol.* **171** 302
[7] Ilic D B 1981 *Rev. Sci. Instrum.* **52** 1542
[8] Bakker L P, Kroesen G M W and de Hoog F J 1999 *IEEE Trans. Plasma Sci.* **27** 759
[9] Kiyokawa K, Matsuoka H, Itou A, Hasegawa K and Sugiyama K 1999 *Surf. Coat. Technol.* **112** 25
[10] Timmermans E A H, Jonkers J, Thomas I A J, Rodero A, Quintero M C, Sola A, Gamero A and van der Mullen J A M 1998 *Spectrochim. Acta* B **53** 1553
[11] Kim Y-H, Choi Y-H, Kim J-H, Park J-K, Ju W-T, Paek K-H and Hwang Y-S 2003 *Surf. Coat. Technol.* **174–175** 535
[12] Straface E, Giacomoni P U and Malorni W 2001 *J. Photochem. Photobiol.* B **63** 52
[13] De Santis L P, Garcia C L, Balajee A S, Latini P, Pichierri P, Nikaido O, Stefanini M and Palitti F 2002 *DNA Repair* **1** 209
[14] Kannan K and Jain S K 2000 *Pathophysiology* **7** 153
[15] Slater J C 1959 *Microwave Transmission* (New York: Dover)
[16] Raizer Y P 1991 *Gas Discharge Physics* (Berlin: Springer)
[17] Jonkers J and Van der Mullen J A M 1999 *J. Quant. Spectrosc. Radiat. Transfer* **61** 703
[18] Jonkers J 1998 *PhD Thesis* Eindhoven University of Technology
[19] Park J, Henins I, Herrmann H W, Selwyn G S and Hicks R F 2001 *J. Appl. Phys.* **89** 20
[20] Lide D R 2003–2004 *Handbook of Chemistry and Physics* vol 84 (Boca Raton, FL: CRC Press)
[21] Foster K R 2000 *IEEE Trans. Plasma Sci*. **28** 15
[22] Pearse R W B and Gaydon A G 1965 *The Identification of Molecular Spectra* (London: Chapman and Hall)
[23] Shi J J, Deng X T, Hall R, Punnett J D and Kong M G 2003 *J. Appl. Phys.* **94** 6303
[24] Laroussi M and Leipold F 2004 *Int. J. Mass Spectrom.* **233** 81